

# Nonlinearity-Driven Morphing and Control of Topological Modes in Non-Hermitian Systems

Zhao-Fan Cai,<sup>1</sup> Yu-Chun Wang,<sup>1</sup> and Tao Liu<sup>1,\*</sup>

<sup>1</sup>*School of Physics and Optoelectronics, South China University of Technology, Guangzhou 510640, China*  
(Dated: November 18, 2024)

Non-Hermitian skin effect (NHSE) and nonlinearity can each delocalize topological zero modes (TZMs) from the boundary. To overcome the challenge of precise parameter tuning imposed by the NHSE-induced delocalization and to enhance the capacity of TZMs limited by nonlinearity-induced partial delocalization in Hermitian systems, we develop non-Hermitian nonlinear topological interface models. This model consists of both Hermitian and non-Hermitian Su-Schrieffer-Heeger (SSH) chains, incorporating nonreciprocal hopping and nonlinearity. When the nonlinearity is applied to both chains, the TZM becomes fully delocalized, extending across the entire lattice of two chains without the need for precise parameter tuning. By adjusting nonlinear coefficients in both chains, the wavefunction profile and plateaus across the entire lattice can be effectively controlled and customized through inherent configuration and intensity of the nonlinearity. Furthermore, the spectral localizer is utilized to demonstrate the topological protection of these extended non-Hermitian TZMs, confirming their robustness against disorder. Their dynamical stability under external pumping is also validated. Our findings provide a deeper insight into how nonlinearity and NHSE affect the behavior of topological modes, opening new possibilities for enhancing their capacity and performance in compact devices.

**Introduction.**—Over the past decade, topological phases have emerged as one of the most rapidly advancing research areas, garnering significant attention across diverse fields such as condensed matters [1–3], photonics [4–6], and electrical circuits systems [7–9]. A hallmark feature of topological phases is the presence of topological modes, typically confined to system boundaries or interfaces and governed by the principle of bulk-boundary correspondence [1]. These topological modes decay exponentially into the bulk and remain resilient to disorder and perturbations, granting them inherent robustness. However, their capacity is limited by the need for bulky materials with sufficiently large lattices in topological applications.

A recent study shows that introducing nonlinearity into the system can overcome this limitation [10]. When combined with topology, the nonlinearity enables various novel topological phenomena, such as emergence of topological soliton states [11–14] and nonlinearity-induced topological phase transitions [15–17]. Furthermore, in this recent study [10], the nonlinearity is employed to partially delocalize the topological zero modes (TZMs), which was originally localized at the interface between a nonlinear Su-Schrieffer-Heeger (SSH) chain and a linear SSH chain, causing the TZMs to spread throughout the entire nonlinear chain. Moreover, the wavefunction profiles of TZMs can be tailored to form arbitrary plateaus [10].

In addition to the nonlinearity, non-Hermitian skin effects (NHSEs) can also contribute to the delocalization of the TZMs [18–20]. The NHSE is characterized by the collapse of bulk-band eigenstates into the localized boundary modes, and its discovery has opened an exciting avenue for exploring unusual physics without

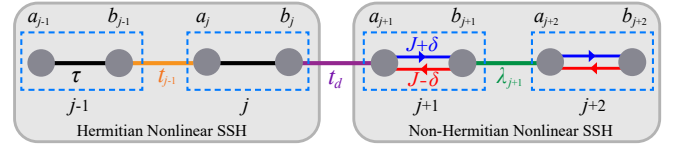


FIG. 1. Tight-binding representation of a one-dimensional topological interface model consisting of a Hermitian nonlinear SSH chain (left) and a non-Hermitian nonlinear SSH chain (right).  $t_{j-1} = \tilde{t}_j + \alpha(|a_j|^2 + |b_{j-1}|^2)$  and  $\lambda_{j+1} = \tilde{\lambda}_j + \beta(|a_{j+2}|^2 + |b_{j+1}|^2)$  are intensity-dependent nonlinear intercell hopping strength in the Hermitian and non-Hermitian chains, respectively. Here,  $\tilde{t}_j$  and  $\tilde{\lambda}_j$  are site-dependent hopping strength,  $\alpha$  and  $\beta$  are Kerr nonlinear coefficients.

Hermitian counterparts in non-Hermitian systems [21–66]. By harnessing the NHSE, the wavefunction of topological zero mode (TZM) can transition from localized to delocalized states when the system parameters satisfy specific conditions [19]. However, the requirement for such precise parameter tuning limits the practical capacity of TZMs.

The above advances in nonlinear and non-Hermitian topologies raise a crucial question: can the combined effects of nonlinearity, NHSE and topology cause the complete delocalization and versatile configuration of topological modes across the entire lattice over a broad range of parameters? Addressing this question is essential for enhancing the capabilities of topological modes and for developing compact and configurable topological devices.

In this work, we explore triple interplay of nonlinearity, NHSE and topology to achieve the delocalization and design of the TZM, which is originally confined to the interface between Hermitian and non-Hermitian SSH

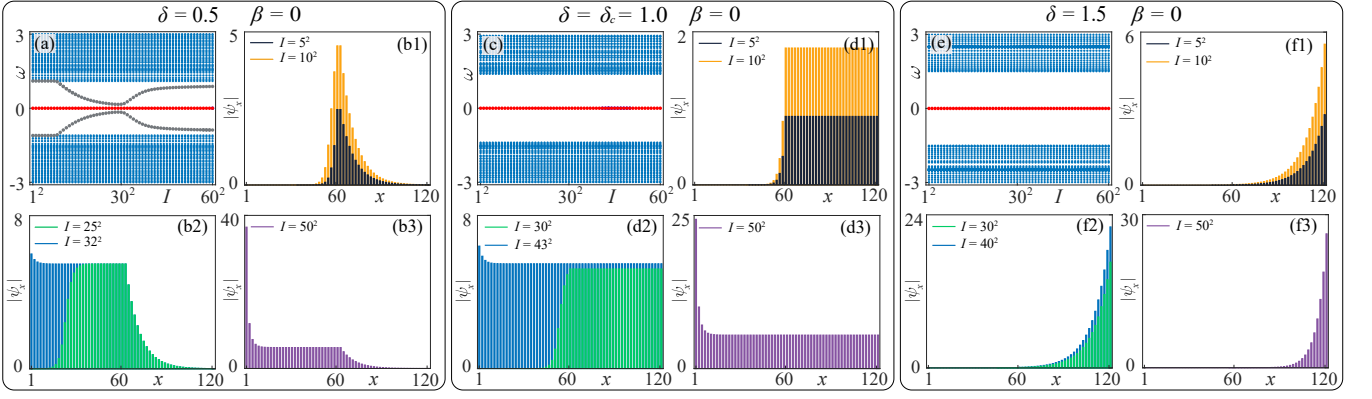


FIG. 2. Eigenfrequency  $\omega$  versus squared amplitude  $I = \sum_j (|a_j|^2 + |b_j|^2)$  for  $\beta = 0$  with (a)  $\delta = 0.5$ , (c)  $\delta = \delta_c = 1.0$ , and (e)  $\delta = 1.5$ , where red dots mark the TZMs. In (a), non-zero in-gap modes (light black dots) are plotted. The corresponding spatial distributions  $|\psi_x| = \langle \psi | \psi \rangle$  of TZMs for different  $I$  are shown in (b1-b3), (d1-d3) and (f1-f3), respectively. Other parameters are used:  $J = 1.5$ ,  $\{\tilde{t}_j\} = 1.0$ ,  $\tau = t_d = \{\tilde{\lambda}_j\} = 2.5$ ,  $\alpha = 0.05$ ,  $n = 31$  and  $L = 121$ .

chains. Notably, when the nonlinearity is applied solely to the Hermitian section of the topological interface model, the TZM can expand across the entire Hermitian chain for small nonreciprocal hopping. As the system approaches a critical threshold, the TZM extends seamlessly over both the Hermitian and non-Hermitian chains. In contrast, with strong nonreciprocal hopping, the NHSE becomes dominant, causing the mode to localize at the chain's boundary. Strikingly, when the nonlinearity is introduced to both the Hermitian and non-Hermitian chains, the TZM achieves full extension across the entire system without requiring precise parameter tuning, thereby greatly enhancing the versatility and capacity of TZMs. Furthermore, this approach allows the wavefunction profiles to be tailored with exceptional flexibility, enabling the creation of custom, arbitrarily shaped configurations across the entire lattice. The topological protection of these extended non-Hermitian TZMs is characterized by the real-space spectral localizer. We also analyze their dynamical stability under external pumping, where an initially localized excitation can evolve into a predefined profile.

**Model.**—We consider a one-dimensional (1D) topological interface model consisting of a Hermitian nonlinear SSH (HN-SSH) chain and a non-Hermitian nonlinear SSH (nHN-SSH) chain, as shown in Fig. 1. Both SSH chains contain two sublattices  $a$  and  $b$ , and their state amplitudes are labeled by  $a_j$  and  $b_j$  on the  $j$ -th unit cell with  $j \leq n$  for HN-SSH chain, and  $j > n$  for nHN-SSH chain. The real-space eigenvector  $|\psi\rangle = (\dots, a_j, b_j, \dots)^T$  of this hybrid system is captured by the nonlinear Schrödinger equation

$$\hat{\mathcal{H}}|\psi\rangle = \omega|\psi\rangle, \quad (1)$$

where  $\omega$  is eigenfrequency, and the tight-binding

Hamiltonian  $\hat{\mathcal{H}}$  is written as

$$\begin{aligned} \hat{\mathcal{H}} = & \sum_{j \leq n} (\tau |a_j\rangle \langle b_j| + t_{j-1} |a_j\rangle \langle b_{j-1}| + \text{H.c.}) \\ & + \sum_{j > n} [(J - \delta) |a_j\rangle \langle b_j| + (J + \delta) |b_j\rangle \langle a_j|] \\ & + \sum_{j > n} (\lambda_j |a_{j+1}\rangle \langle b_j| + \text{H.c.}) \\ & + t_d (|a_{n+1}\rangle \langle b_n| + \text{H.c.}). \end{aligned} \quad (2)$$

In Eq. (2),  $\tau$  is intracell hopping strength in the HN-SSH chain (see Fig. 1), and  $t_j = \tilde{t}_j + \alpha(|a_{j+1}|^2 + |b_j|^2)$  is intensity-dependent nonlinear intercell hopping strength, with  $\alpha$  being Kerr nonlinear coefficient.  $J \pm \delta$  denote the nonreciprocal intracell hopping amplitudes in the nHN-SSH chain, and  $\lambda_j = \tilde{\lambda}_j + \beta(|a_{j+1}|^2 + |b_j|^2)$  is the nonlinear intercell hopping strength.  $t_d$  represents the inter-chain coupling strength.

**Nonlinear and non-Hermitian morphing of TZMs.**—In absence of nonlinearity with  $\alpha = \beta = 0$ , a TZM can be delocalized from the interference, and becomes an extended state occupying the entire non-Hermitian SSH chain at a critical value with  $\delta_c = \lambda - J$  [19]. Here, we will show that the TZM can occupy the entire Hermitian and non-Hermitian chains when the nonlinearity is applied to the Hermitian chain with  $\alpha \neq 0$  and  $\beta = 0$ . In order to demonstrate this, we solve self-consistently the nonlinear equation in Eq. (1) for different squared amplitudes  $I = \sum_j (|a_j|^2 + |b_j|^2)$ . Figure 2 shows eigenfrequency spectrum  $\omega$  versus  $I$ , and the corresponding spatial distributions  $|\psi_x| = \langle \psi | \psi \rangle$  ( $x$  denotes lattice site) of TZMs [red dots in Fig. 2(a,c,e)] for different asymmetrical hopping parameter  $\delta$  with  $\alpha = 0.05$  and  $\beta = 0$ . Note that, in addition to TZMs, the nonlinearity can induce non-zero in-gap modes [see light black dots in Fig. 2(a)]. In this work, our primary focus is on TZMs, and thus we exclusively plot the in-gap zero modes below. Detailed

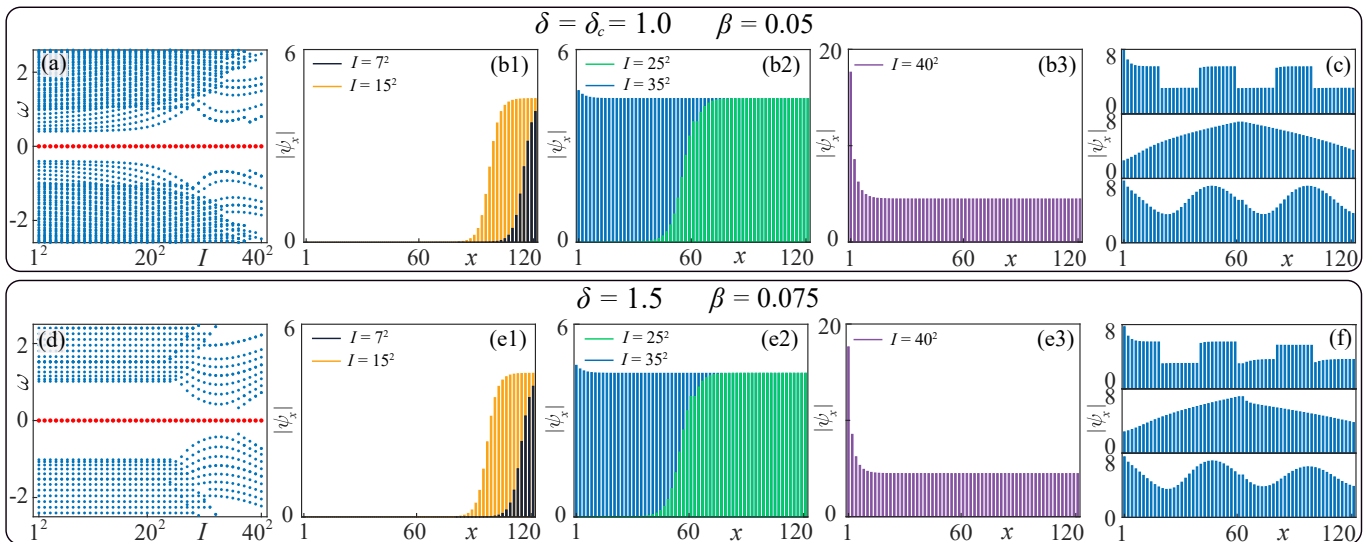


FIG. 3.  $\omega$  versus  $I$  (a) for  $\delta = \delta_c = 1$  and  $\beta = 0.05$ , and (b) for  $\delta = 1.5$  and  $\beta = 0.075$ , where red dots mark the TZMs. The corresponding spatial distributions  $|\psi_x|$  of TZMs for different  $I$ , with  $\{\tilde{t}_j\} = \{\tilde{\lambda}_j\} = 1.5$ , are shown in (b1-b3) and (e1-e3), respectively. Square, isosceles triangle and cosine profiles of TZMs (c) for  $\delta = \delta_c = 1$  and  $\beta = 0.05$ , and (f) for  $\delta = 1.5$  and  $\beta = 0.075$  by designing  $\{\tilde{t}_j\}$  and  $\{\tilde{\lambda}_j\}$ , where the corresponding distributions  $\{\tilde{t}_j\}$  and  $\{\tilde{\lambda}_j\}$  are provided in SM [67]. Other parameters are used:  $J = 1.5$ ,  $\alpha = 0.05$ ,  $\tau = t_d = 2.5$ ,  $n = 31$  and  $L = 121$ .

discussions of the non-zero in-gap modes for various values of  $I$  are provided in the Sec. I of the Supplemental Material (SM) [67].

For  $\delta = 0.5$ , which is below the critical value  $\delta_c$ , a TZM is localized at the interface between topologically nontrivial NH-SSH chain and the trivial non-Hermitian linear chain when  $I$  is small, as shown in Fig. 2(b1). As  $I$  increases, the TZM becomes increasingly delocalized toward the NH-SSH chain, and eventually spreads uniformly across the entire Hermitian chain at large values of  $I$ , e.g.,  $I = 32^2$  [see Fig. 2(b2)]. Furthermore, as  $I$  increases further, the TZM is compressed toward the left boundary while maintaining a plateau in the bulk region of the Hermitian lattice at significantly large values of  $I$ , e.g.,  $I = 50^2$  [see Fig. 2(b3)]. Note that the same nonlinearity-induced delocalization of TZMs is also observed in the Hermitian case with  $\delta = 0$  [10].

Interesting results occur when  $\delta = \delta_c$ . For small values of  $I$  with the weak nonlinearity, the TZM occupies the whole non-Hermitian chain due to the competition between NHSE localization and topological localization of the in-gap interface state [19], as shown in Fig. 2(d1). However, as  $I$  increases, the TZM gradually spreads to uniformly occupy the entire Hermitian and non-Hermitian lattices due to the triple interplay of the nonlinearity, NHSE and topology at large values of  $I$ , e.g.,  $I = 43^2$  [see Fig. 2(d2)]. Furthermore, for significantly large values of  $I$ , e.g.,  $I = 50^2$  in Fig. 2(d3), the TZM is compressed toward the left boundary while maintaining a plateau throughout the entire bulk region of two chains.

In the case of strong nonreciprocal hopping with, e.g.,  $\delta = 1.5$ , the NHSE dominates the nonlinear effects, and the TZM is localized at the right boundary even for large values of  $I$ , as shown in Fig. 2(f1-f3). These results show that the triple interplay of nonlinearity, nonreciprocal hopping and topology determines the morphing of TZM wavefunction.

*Nonlinearity-enabled control of TZMs.*—As shown above, the TZM can occupy the entire lattice when  $\delta = \delta_c$  with  $\beta = 0$ , which can benefit a wide variety of topological applications [19]. However, the necessary condition with  $\delta_c = \lambda - J$  in the non-Hermitian linear chain restricts its tunability. To overcome this limitation, we introduce nonlinearity into the non-Hermitian chain, i.e.,  $\beta \neq 0$  in the Hamiltonian  $\hat{H}$  in Eq. (2).

Figure 3 shows the eigenfrequency  $\omega$  versus  $I$ , and the corresponding spatial distributions  $|\psi_x|$  of TZMs [red dots in Fig. 3(a,d)] for  $\delta = \delta_c$  with  $\beta = 0.05$  [see Fig. 3(b1-b3)], and  $\delta = 1.5$  with  $\beta = 0.075$  [see Fig. 3(e1-e3)]. When  $\delta = \delta_c$ , in contrast to the case of the non-Hermitian linear chain [see Fig. 2(d1)], the TZM is initially localized at the right boundary due to NHSE, and then gradually spreads from the boundary as  $I$  increases [see Fig. 3(b1)]. For the large values of  $I$ , the TZM occupies the entire lattice [see Fig. 3(b2-b3)]. The most notable finding is that the delocalization of TZMs, accompanied by the occupation of the entire lattice, occurs without requiring  $\delta = \delta_c$  for  $\beta \neq 0$ . For example, even with unidirectional hopping at  $\delta = 1.5$ , a uniform distribution of TZMs across the entire lattice is observed [see Fig. 3(e2)], which does not occur for  $\beta = 0$ .

Along the entire lattice, arbitrary wavefunction profiles of TZMs can be achieved by designing site-dependent hopping parameters,  $\{\tilde{t}_j\}$  and  $\{\tilde{\lambda}_j\}$ , without requiring  $\delta = \delta_c$  for  $\beta \neq 0$ . Figures 3(c) and (f) illustrate square, isosceles triangle, and cosine profiles of TZMs for  $\delta = \delta_c = 1$  and  $\delta = 1.5$ , respectively. Notably, even when  $\delta$  exceeds the critical value  $\delta_c$ , ideal wavefunction profiles can still be achieved by adjusting  $\beta$ , as demonstrated by comparing Figs. 3(c) and 3(f). Note that the wavefunction profiles of TZMs for  $\delta$  below  $\delta_c$  are provided in the Sec. II of the SM [67].

*Topological origin of zero modes.*—Conventional topological invariants are typically characterized by the system's band structure and associated Bloch eigenstates, and are regarded as global properties of the system. However, nonlinear effects are inherently local, and strong nonlinearity breaks translation symmetry, rendering topological invariants in momentum space ill-defined. To verify the topological origin of the zero modes in our nonlinear non-Hermitian system, we utilize a spectral localizer [68–71], which is applicable to systems lacking translation symmetry. In order to employ the spectral localizer to our non-Hermitian system (see details in the Sec. III of the SM [67]), we map the non-Hermitian Hamiltonian  $\hat{\mathcal{H}}$  to the Hermitian one  $\hat{\mathcal{H}}_S$  via a similarity transformation  $\hat{S}$ , i.e.,  $\hat{\mathcal{H}}_S = \hat{S}\hat{\mathcal{H}}\hat{S}^{-1}$ , with its eigenvector satisfying  $|\bar{\psi}\rangle = \hat{S}|\psi\rangle$ . The spectral localizer of a 1D system at any choice of location  $x$  and frequency  $\bar{\omega}$  is written as [71]

$$L_{\zeta \equiv (x, \bar{\omega})}(\hat{X}, \hat{\mathcal{H}}_S) = \eta(\hat{X} - x\mathbf{I}) \otimes \Gamma_x + (\hat{\mathcal{H}}_S - \bar{\omega}) \otimes \Gamma_y, \quad (3)$$

where  $\Gamma_x$  and  $\Gamma_y$  are Pauli matrices,  $\mathbf{I}$  is an identity matrix,  $\eta$  is a tuning parameter which ensures  $\hat{X}$  and  $\hat{\mathcal{H}}_S$  have compatible units, and  $\hat{X}$  is a diagonal matrix whose entries correspond to the coordinates of each lattice site. When the system preserves the chiral symmetry, the spectral localizer can be written in a reduced form [71] as  $\tilde{L}_{\zeta \equiv (x, \bar{\omega})}(\hat{X}, \hat{\mathcal{H}}_S) = \eta(\hat{X} - x\mathbf{I})\hat{\Pi} + \hat{\mathcal{H}}_S - i\bar{\omega}\hat{\Pi}$ , with  $\hat{\Pi}$  being the system's chiral operator. The eigenvalue of  $\tilde{L}_{\zeta}$  is labeled by  $\sigma(\tilde{L}_{\zeta})$ , and the local band gap is given by the smallest value as  $\mu_{\zeta} = \left| \sigma_{\min}(\tilde{L}_{\zeta}) \right|$ . Furthermore, the local topological invariant is written by [71]

$$C_{\zeta} = \frac{1}{2} \text{Sig}(\tilde{L}_{\zeta}(\hat{X}, \hat{\mathcal{H}}_S)), \quad (4)$$

where Sig is the signature of a matrix, i.e., its number of positive eigenvalues minus its number of negative ones.

Figure 4 shows spatial distributions  $|\bar{\psi}_x| = |\hat{S}\psi_x|$  of TZMs after a similarity transformation  $\hat{S}$ , site-resolved  $\sigma(\tilde{L}_{\zeta})$ ,  $C_{\zeta}$ , and  $\mu_{\zeta}$  for different  $I$  at  $\bar{\omega} = 0$  with  $\delta = 1$  and  $\beta = 0.05$ . Specifically,  $\sigma(\tilde{L}_{\zeta})$ ,  $C_{\zeta}$ , and  $\mu_{\zeta}$  exhibit intensity dependence. Whenever  $\sigma(\tilde{L}_{\zeta})$  crosses zero [see red curves in Fig. 4(d-f)], the value

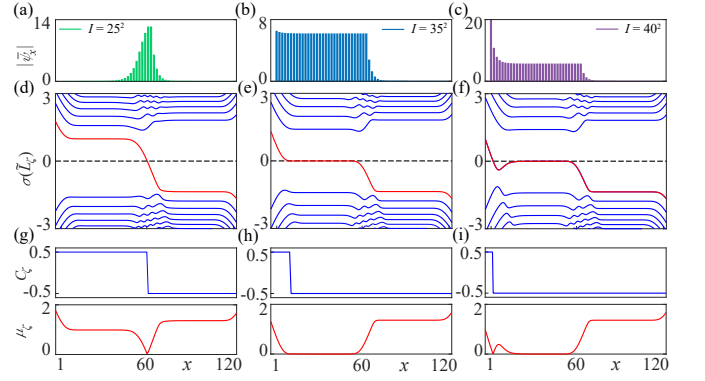


FIG. 4. (a-c) Spatial distributions  $|\bar{\psi}_x| = |\hat{S}\psi_x|$  of TZMs. (d-f)  $\sigma(\tilde{L}_{\zeta})$  versus  $x$  for different  $I$  with  $\eta = 0.2$  and  $\bar{\omega} = 0$ . (g-i) Site-resolved  $C_{\zeta}$  and  $\mu_{\zeta}$  for different  $I$ . The distributions  $\{\tilde{t}_j\}$  and  $\{\tilde{\lambda}_j\}$  and other parameters are chosen as the same as the case of  $\delta = 1$  and  $\beta = 0.05$  in Fig. 3.

of  $C_{\zeta}$  change accordingly [see blue curves in Fig. 4(g-i)]. Simultaneously, the local gap of  $\mu_{\zeta}$  closes [see red curves in Fig. 4(g-i)]. The fact that a zero value of  $\sigma(\tilde{L}_{\zeta})$  at  $\zeta = \{x_0, 0\}$  signifies a zero-frequency mode that is localized near at  $x_0$ , implies that the change in  $C_{\zeta}$  at  $\zeta = \{x_0, 0\}$  reflects the bulk-boundary correspondence. Due to the topological protection revealed by the spectral localizer, these extended TZMs are resilient to disorders, as demonstrated in the SM [67].

*Dynamical evolution under external pumping.*—Unlike conventional linear topological models, nonlinear models can exhibit distinctive dynamical properties that depend on how intensity levels are reached, enabling intrinsic control on TZMs through external pumping [10]. Here, we investigate the dynamical evolution under an external pumping scheme, as illustrated in Fig. 5(a), with the evolution governed by the following equation:

$$\frac{\partial |\Phi\rangle}{\partial t} = -i(\hat{\mathcal{H}} + \hat{\mathcal{H}}_{\text{loss}})|\Phi\rangle + \xi|S\rangle e^{-i\bar{\omega}t}, \quad (5)$$

where  $\hat{\mathcal{H}}_{\text{loss}} = \sum_j (-i\kappa_a |a_j\rangle \langle a_j| - i\kappa_b |b_j\rangle \langle b_j|)$ , denotes onsite losses in the two sublattices, which contributes to stabilizing excitation. The pumping sources  $|S\rangle \equiv (0, \dots, S_j, \dots)^T$  are only applied to the  $a$ -sites of the non-Hermitian chain [see Fig. 5(a)], with the pumping frequency denoted by  $\bar{\omega}$ , and the pumping strength  $\xi$ . We consider a single external pumping source with the distribution  $\{S_j\} = \delta_{j,1}$  with  $\bar{\omega} = 0$ . A complementary discussion on the alternative distribution for  $\{S_j\}$  is provided in the SM [67].

Figure 5(b) plots the intensity  $|\Phi|^2$  of the evolved steady state versus  $\xi$ , with the wavefunction profile  $|\text{Re}(\Phi_x)|$  for different  $\xi$  shown in Fig. 5(c). As the pumping strength  $\xi$  increases, an initially localized waveform begins to spread and gradually occupies the non-Hermitian chain [see green line in Fig. 5(c)].

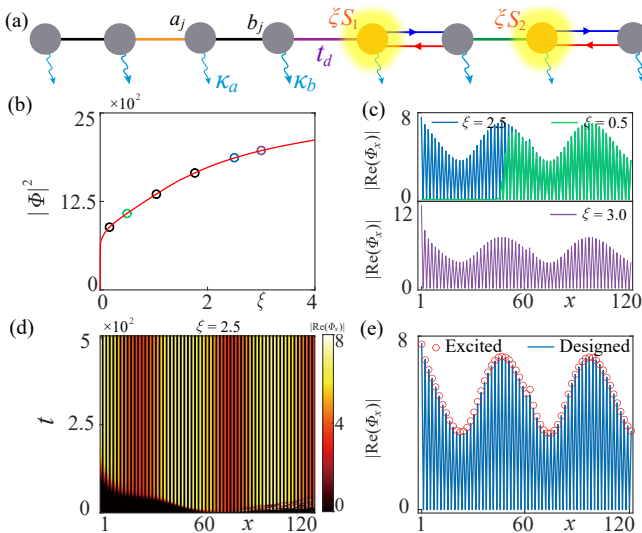


FIG. 5. (a) Schematic showing external pumping applied to the  $a$ -sites of the non-Hermitian chain, highlighted by yellow spots. The intensity distributions of pumping sources are represented by  $\{\xi S_j\}$ , with  $\xi$  being pumping strength. The cyan wave arrows indicate onsite losses in the two sublattices, labeled  $\kappa_a$  and  $\kappa_b$ . (b) Intensity  $|\Phi|^2$  of the evolved steady state versus  $\xi$ . The circles represent results from the evolution equation (5), which closely match the outcomes from self-consistent nonlinear equations (red curve) in the SM [67]. (c) Wavefunction profile  $|\text{Re}(\Phi_x)|$  of steady states for different  $\xi$ . (d) Time- and space-resolved  $|\text{Re}(\Phi_x)|$  for  $\xi = 4.5$ , with the steady-state result highlighted by red circles in (e). In (e), the steady wavefunction profile closely matches the designed one (blue line) of the TZM. The parameters are the same as the case of  $\delta = 1$  and  $\beta = 0.05$  in Fig. 3, with  $\tilde{\omega} = 0$ ,  $\kappa_a = 0.01$  and  $\kappa_b = 0.5$ .

Eventually, this expansion allows the waveform to fill the entire lattice of both the Hermitian and non-Hermitian chains, aligning with the designed profile (indicated by the blue line). Upon further increasing  $\xi$ , the steady-state intensity becomes concentrated toward the left boundary while maintaining the plateau in the bulk region (illustrated by the purple line). Comparing the steady-state wavefunction profile (see red circles in Fig. 5(e)) with the designed target profile (blue lines) of the TZM shows a close match. A detailed discussion on the evolution into various designed wavefunction profiles is provided in the SM [67]. These results demonstrate that, by leveraging dynamical evolution, we can achieve arbitrarily desired waveform across the entire lattice.

*Conclusion.*—In summary, we demonstrate the nonlinear- and non-Hermitian-driven morphing and arbitrary design of wavefunction profiles across the entire lattice of a topological interface mode, composed of both Hermitian and non-Hermitian SSH chains. Unlike the delocalization induced by NHSE under critical conditions or the partial delocalization caused by nonlinearity in Hermitian systems, the triple interplay

of nonlinearity, NHSE and topology fully delocalize the TZM, spreading it across the entire lattice of both chains without the need for precision parameter tuning. The arbitrary waveform of the TZM can be tailored by adjusting the nonlinearity in both chains, with these extended non-Hermitian TZMs showing significant robustness against disorder and maintaining dynamical stability.

T.L. acknowledges the support from the National Natural Science Foundation of China (Grant No. 12274142), the Fundamental Research Funds for the Central Universities (Grant No. 2023ZYGXZR020), Introduced Innovative Team Project of Guangdong Pearl River Talents Program (Grant No. 2021ZT09Z109), and the Startup Grant of South China University of Technology (Grant No. 20210012).

\* E-mail: liutao0716@scut.edu.cn

- [1] M. Z. Hasan and C. L. Kane, “Colloquium: Topological insulators,” *Rev. Mod. Phys.* **82**, 3045 (2010).
- [2] X.-L. Qi and S.-C. Zhang, “Topological insulators and superconductors,” *Rev. Mod. Phys.* **83**, 1057 (2011).
- [3] C.-K. Chiu, J. C. Y. Teo, A. P. Schnyder, and S. Ryu, “Classification of topological quantum matter with symmetries,” *Rev. Mod. Phys.* **88**, 035005 (2016).
- [4] L. Lu, J. D. Joannopoulos, and M. Soljačić, “Topological photonics,” *Nat. Photonics* **8**, 821 (2014).
- [5] T. Ozawa, H. M. Price, A. Amo, N. Goldman, M. Hafezi, L. Lu, M. C. Rechtsman, D. Schuster, J. Simon, O. Zilberberg, and I. Carusotto, “Topological photonics,” *Rev. Mod. Phys.* **91**, 015006 (2019).
- [6] C. Leefmans, A. Dutt, J. Williams, L. Yuan, M. Parto, F. Nori, S. Fan, and A. Marandi, “Topological dissipation in a time-multiplexed photonic resonator network,” *Nat. Phys.* **18**, 442 (2022).
- [7] S. Imhof, C. Berger, F. Bayer, J. Brehm, L. W. Molenkamp, T. Kiessling, F. Schindler, C. H. Lee, M. Greiter, T. Neupert, and R. Thomale, “Topoelectrical-circuit realization of topological corner modes,” *Nat. Phys.* **14**, 925 (2018).
- [8] C. H. Lee, S. Imhof, C. Berger, F. Bayer, J. Brehm, L. W. Molenkamp, T. Kiessling, and R. Thomale, “Topoelectrical Circuits,” *Commun. Phys.* **1** (2018), 10.1038/s42005-018-0035-2.
- [9] H. Yang, L. Song, Y. Cao, and P. Yan, “Circuit realization of topological physics,” *Phys. Rep.* **1093**, 1 (2024).
- [10] K. Bai, J.-Z. Li, T.-R. Liu, L. Fang, D. Wan, and M. Xiao, “Arbitrarily configurable nonlinear topological modes,” *Phys. Rev. Lett.* **133**, 116602 (2024).
- [11] Y. Lumer, Y. Plotnik, M. C. Rechtsman, and M. Segev, “Self-Localized States in Photonic Topological Insulators,” *Phys. Rev. Lett.* **111**, 243905 (2013).
- [12] D. Leykam and Y. D. Chong, “Edge Solitons in Nonlinear-Photonic Topological Insulators,” *Phys. Rev. Lett.* **117**, 143901 (2016).
- [13] S. Mukherjee and M. C. Rechtsman, “Observation of Unidirectional Solitonlike Edge States in Nonlinear

- Floquet Topological Insulators,” *Phys. Rev. X* **11**, 041057 (2021).
- [14] S. Mukherjee and M. C. Rechtsman, “Observation of Floquet solitons in a topological bandgap,” *Science* **368**, 856 (2020).
- [15] F. Zangeneh-Nejad and R. Fleury, “Nonlinear Second-Order Topological Insulators,” *Phys. Rev. Lett.* **123**, 053902 (2019).
- [16] T. Tuloup, R. W. Bomantara, C. H. Lee, and J. Gong, “Nonlinearity induced topological physics in momentum space and real space,” *Phys. Rev. B* **102**, 115411 (2020).
- [17] K. Sone, M. Ezawa, Y. Ashida, N. Yoshioka, and T. Sagawa, “Nonlinearity-induced topological phase transition characterized by the nonlinear Chern number,” *Nat. Phys.* **20**, 1164 (2024).
- [18] P. Gao, M. Willatzen, and J. Christensen, “Anomalous topological edge states in non-Hermitian piezophononic media,” *Phys. Rev. Lett.* **125**, 206402 (2020).
- [19] W. Wang, X. Wang, and G. Ma, “Non-Hermitian morphing of topological modes,” *Nature* **608**, 50 (2022).
- [20] W. Zhu, W. X. Teo, L. Li, and J. Gong, “Delocalization of topological edge states,” *Phys. Rev. B* **103**, 195414 (2021).
- [21] T. Gao, E. Estrecho, K. Y. Bliokh, T. C. H. Liew, M. D. Fraser, S. Brodbeck, M. Kamp, C. Schneider, S. Höfling, Y. Yamamoto, F. Nori, Y. S. Kivshar, A. G. Truscott, R. G. Dall, and E. A. Ostrovskaya, “Observation of non-Hermitian degeneracies in a chaotic exciton-polariton billiard,” *Nature* **526**, 554 (2015).
- [22] F. Monifi, J. Zhang, Ş. K. Özdemir, B. Peng, Y.-x. Liu, F. Bo, F. Nori, and L. Yang, “Optomechanically induced stochastic resonance and chaos transfer between optical fields,” *Nat. Photon.* **10**, 399 (2016).
- [23] J. Zhang, B. Peng, Ş. K. Özdemir, K. Pichler, D. O. Krimer, G. Zhao, F. Nori, Y.-x. Liu, S. Rotter, and L. Yang, “A phonon laser operating at an exceptional point,” *Nat. Photon.* **12**, 479 (2018).
- [24] Y. Xu, S. T. Wang, and L. M. Duan, “Weyl exceptional rings in a three-dimensional dissipative cold atomic gas,” *Phys. Rev. Lett.* **118**, 045701 (2017).
- [25] Z. Gong, Y. Ashida, K. Kawabata, K. Takasan, S. Higashikawa, and M. Ueda, “Topological phases of non-Hermitian systems,” *Phys. Rev. X* **8**, 031079 (2018).
- [26] B. Peng, S. K. Özdemir, S. Rotter, H. Yilmaz, M. Liertzer, F. Monifi, C. M. Bender, F. Nori, and L. Yang, “Loss-induced suppression and revival of lasing,” *Science* **346**, 328 (2014).
- [27] R. El-Ganainy, K. G. Makris, M. Khajavikhan, Z. H. Musslimani, S. Rotter, and D. N. Christodoulides, “Non-Hermitian physics and PT symmetry,” *Nat. Phys.* **14**, 11 (2018).
- [28] S. Yao and Z. Wang, “Edge states and topological invariants of non-Hermitian systems,” *Phys. Rev. Lett.* **121**, 086803 (2018).
- [29] K. Zhang, Z. Yang, and C. Fang, “Correspondence between winding numbers and skin modes in non-Hermitian systems,” *Phys. Rev. Lett.* **125**, 126402 (2020).
- [30] K. Yokomizo and S. Murakami, “Non-Bloch band theory of non-Hermitian systems,” *Phys. Rev. Lett.* **123**, 066404 (2019).
- [31] S. Yao, F. Song, and Z. Wang, “Non-Hermitian Chern bands,” *Phys. Rev. Lett.* **121**, 136802 (2018).
- [32] F. K. Kunst, E. Edvardsson, J. C. Budich, and E. J. Bergholtz, “Biorthogonal bulk-boundary correspondence in non-Hermitian systems,” *Phys. Rev. Lett.* **121**, 026808 (2018).
- [33] L. Tao, Y.-R. Zhang, Q. Ai, Z. Gong, K. Kawabata, M. Ueda, and F. Nori, “Second-order topological phases in non-Hermitian systems,” *Phys. Rev. Lett.* **122**, 076801 (2019).
- [34] F. Song, S. Yao, and Z. Wang, “Non-Hermitian skin effect and chiral damping in open quantum systems,” *Phys. Rev. Lett.* **123**, 170401 (2019).
- [35] J. Y. Lee, J. Ahn, H. Zhou, and A. Vishwanath, “Topological correspondence between Hermitian and non-Hermitian systems: Anomalous dynamics,” *Phys. Rev. Lett.* **123**, 206404 (2019).
- [36] K. Kawabata, T. Bessho, and M. Sato, “Classification of exceptional points and non-Hermitian topological semimetals,” *Phys. Rev. Lett.* **123**, 066405 (2019).
- [37] L. Li, C. H. Lee, and J. Gong, “Topological switch for non-Hermitian skin effect in cold-atom systems with loss,” *Phys. Rev. Lett.* **124**, 250402 (2020).
- [38] L. Li, C. H. Lee, S. Mu, and J. Gong, “Critical non-Hermitian skin effect,” *Nat. Commun.* **11**, 5491 (2020).
- [39] N. Okuma, K. Kawabata, K. Shiozaki, and M. Sato, “Topological origin of non-Hermitian skin effects,” *Phys. Rev. Lett.* **124**, 086801 (2020).
- [40] Y. Yi and Z. Yang, “Non-Hermitian skin modes induced by on-site dissipations and chiral tunneling effect,” *Phys. Rev. Lett.* **125**, 186802 (2020).
- [41] Z. Y. Ge, Y. R. Zhang, T. Liu, S. W. Li, H. Fan, and F. Nori, “Topological band theory for non-Hermitian systems from the Dirac equation,” *Phys. Rev. B* **100**, 054105 (2019).
- [42] H. Zhou and J. Y. Lee, “Periodic table for topological bands with non-Hermitian symmetries,” *Phys. Rev. B* **99**, 235112 (2019).
- [43] H. Zhao, X. Qiao, T. Wu, B. Midya, S. Longhi, and L. Feng, “Non-Hermitian topological light steering,” *Science* **365**, 1163 (2019).
- [44] K. Kawabata, K. Shiozaki, M. Ueda, and M. Sato, “Symmetry and topology in non-Hermitian physics,” *Phys. Rev. X* **9**, 041015 (2019).
- [45] D. S. Borgnia, A. J. Kruchkov, and R.-J. Slager, “Non-Hermitian boundary modes and topology,” *Phys. Rev. Lett.* **124**, 056802 (2020).
- [46] T. Liu, J. J. He, T. Yoshida, Z.-L. Xiang, and F. Nori, “Non-Hermitian topological Mott insulators in one-dimensional fermionic superlattices,” *Phys. Rev. B* **102**, 235151 (2020).
- [47] K. Y. Bliokh, D. Leykam, M. Lein, and F. Nori, “Topological non-Hermitian origin of surface Maxwell waves,” *Nat. Comm.* **10**, 580 (2019).
- [48] K. Yokomizo and S. Murakami, “Scaling rule for the critical non-Hermitian skin effect,” *Phys. Rev. B* **104**, 165117 (2021).
- [49] H. Jiang and C. H. Lee, “Dimensional transmutation from non-Hermiticity,” *Phys. Rev. Lett.* **131**, 076401 (2023).
- [50] T. Liu, J. J. He, Z. Yang, and F. Nori, “Higher-order Weyl-exceptional-ring semimetals,” *Phys. Rev. Lett.* **127**, 196801 (2021).
- [51] E. J. Bergholtz, J. C. Budich, and F. K. Kunst, “Exceptional topology of non-Hermitian systems,” *Rev. Mod. Phys.* **93**, 015005 (2021).

- [52] Y. Li, C. Liang, C. Wang, C. Lu, and Y.-C. Liu, “Gain-loss-induced hybrid skin-topological effect,” *Phys. Rev. Lett.* **128**, 223903 (2022).
- [53] Q. Wang, C. Zhu, X. Zheng, H. Xue, B. Zhang, and Y. D. Chong, “Continuum of bound states in a non-Hermitian model,” *Phys. Rev. Lett.* **130**, 103602 (2023).
- [54] K. Zhang, Z. Yang, and C. Fang, “Universal non-Hermitian skin effect in two and higher dimensions,” *Nat. Commun.* **13** (2022), 10.1038/s41467-022-30161-6.
- [55] M. Parto, C. Leefmans, J. Williams, F. Nori, and A. Marandi, “Non-Abelian effects in dissipative photonic topological lattices,” *Nat. Comm.* **14**, 1440 (2023).
- [56] Z. Ren, D. Liu, E. Zhao, C. He, K. K. Pak, J. Li, and G.-B. Jo, “Chiral control of quantum states in non-Hermitian spin-orbit-coupled fermions,” *Nat. Phys.* **18**, 385 (2022).
- [57] K. Kawabata, T. Numasawa, and S. Ryu, “Entanglement phase transition induced by the non-Hermitian skin effect,” *Phys. Rev. X* **13**, 021007 (2023).
- [58] C.-A. Li, B. Trauzettel, T. Neupert, and S.-B. Zhang, “Enhancement of second-order non-Hermitian skin effect by magnetic fields,” *Phys. Rev. Lett.* **131**, 116601 (2023).
- [59] J. Liu, Z.-F. Cai, T. Liu, and Z. Yang, “Reentrant non-Hermitian skin effect in coupled non-Hermitian and Hermitian chains with correlated disorder,” [arXiv:2311.03777](https://arxiv.org/abs/2311.03777) (2023).
- [60] Z.-F. Cai, T. Liu, and Z. Yang, “Non-Hermitian skin effect in periodically driven dissipative ultracold atoms,” *Phys. Rev. A* **109**, 063329 (2024).
- [61] X. Li, J. Liu, and T. Liu, “Localization-delocalization transitions in non-Hermitian Aharonov-Bohm cages,” *Front. Phys.* **19**, 33211 (2024).
- [62] H.-Y. Wang, F. Song, and Z. Wang, “Amoeba formulation of non-Bloch band theory in arbitrary dimensions,” *Phys. Rev. X* **14**, 021011 (2024).
- [63] K. Zhang, C. Fang, and Z. Yang, “Dynamical degeneracy splitting and directional invisibility in non-Hermitian systems,” *Phys. Rev. Lett.* **131**, 036402 (2023).
- [64] Y.-M. Hu, H.-Y. Wang, Z. Wang, and F. Song, “Geometric origin of non-Bloch  $\mathcal{PT}$  symmetry breaking,” *Phys. Rev. Lett.* **132**, 050402 (2024).
- [65] C. R. Leefmans, M. Parto, J. Williams, G. H. Y. Li, A. Dutt, F. Nori, and A. Marandi, “Topological temporally mode-locked laser,” *Nat. Phys.* **20**, 852 (2024).
- [66] M. Yang and C. H. Lee, “Percolation-induced  $\mathcal{PT}$  symmetry breaking,” *Phys. Rev. Lett.* **133**, 136602 (2024).
- [67] See Supplemental Material for detailed derivations.
- [68] A. Cerjan and T. A. Loring, “Local invariants identify topology in metals and gapless systems,” *Phys. Rev. B* **106**, 064109 (2022).
- [69] K. Y. Dixon, T. A. Loring, and A. Cerjan, “Classifying topology in photonic heterostructures with gapless environments,” *Phys. Rev. Lett.* **131**, 213801 (2023).
- [70] S. Wong, T. A. Loring, and A. Cerjan, “Probing topology in nonlinear topological materials using numerical  $k$ -theory,” *Phys. Rev. B* **108**, 195142 (2023).
- [71] W. Cheng, A. Cerjan, S.-Y. Chen, E. Prodan, T. A. Loring, and C. Prodan, “Revealing topology in metals using experimental protocols inspired by  $k$ -theory,” *Nat. Commun.* **14**, 3071 (2023).